Fiber push-out testing apparatus for elevated temperatures

Jeffrey I. Eldridge and Ben T. Ebihara
NASA Lewis Research Center, Cleveland, Ohio 44135

(Received 17 March 1993; accepted 22 November 1993)

A newly developed apparatus has been designed for performing fiber push-out testing on continuous fiber-reinforced composites at elevated temperatures. This test measures the force at which a fiber resists being pushed by a flat-bottomed indenter moving at a constant speed. The applied load versus time curve characterizes the fiber debonding and sliding behavior. Extending measurements to elevated temperatures required incorporating sample/indenter heating in a nonoxidizing environment. With this new apparatus, fiber push-out tests have been performed up to 1100 °C in a vacuum of 10^{-6} Torr. A line-of-sight to the sample is maintained during the test which allows video monitoring of the push-out process. Results are shown for SCS-6 SiC fiber-reinforced Ti–24Al–11Nb (at. %) and Ti–15V–3Cr–3Sn–3Al (at. %) matrix composites. The results are discussed in terms of residual stresses, interfacial wear, matrix ductility, and changing modes of interfacial failure. The effect of temperature-dependent interfacial wear on the interfacial roughness contribution to frictional shear stresses during fiber sliding is examined.

I. INTRODUCTION

Fiber push-out testing has become an important tool for characterizing fiber debonding and sliding behavior in fiber-reinforced composite materials.[1–7] This interfacial behavior is important because it has a significant impact on the overall strength and toughness of the composite. Various models have been proposed which relate the mechanical properties of the interface to those of the composite.[8,9] In addition to fiber push-out testing, several other methods have been used to evaluate mechanical properties of the fiber/matrix interface. These include fiber pull-out,[10,11] fiber fragmentation,[12] matrix cracking,[13] and fiber/matrix displacements due to thermal cycling.[14] While each of these methods has its advantages, none of them directly measures the dynamic response to mechanical loading except for fiber push-out and pull-out.

There are counterbalancing benefits and drawbacks to consider in deciding between fiber push-out and pull-out testing. Fiber pull-out testing has the advantage of more closely duplicating the stress states at the interface present in a composite under tension; however, it requires sample geometries which can be extremely difficult to prepare and which produce only one measurement per specimen.[11] This difficult sample preparation makes routine measurements and accumulation of statistical distributions virtually impossible for many composite systems. In contrast, fiber push-out testing is conducive to more routine testing and generates many measurements per specimen, and thus, was chosen as the testing procedure for this paper.

Because the targeted use of many of the composite materials is at elevated temperatures, the benefits of extending these measurements to elevated temperatures are clear: (i) to generate data at composite service temperatures that could be used to optimize interfacial mechanical behavior at those temperatures and (ii) to evaluate the effects of residual stresses on fiber debonding and sliding. To date, however, almost all reported fiber push-out tests have been performed at room temperature. An exception is the work of Morscher *et al.*[15] who used a modified high-temperature microhardness tester to perform elevated temperature push-outs. This work demonstrated general trends in the temperature dependence of fiber debonding and sliding; however, the testing was limited to dead-weight loading, which makes accurate determination of debonding and sliding loads impossible. Also, the test was not monitored visually. The lack of real-time visual monitoring necessitated the use of pointed indenters, which can be used only for very short fiber displacements and make fiber damage more likely. Some of these limitations were overcome by Brun[16] who modified a hot hardness tester by replacing dead-weight loading with motor-driven continuous loading. Also, a flat-bottomed conical indenter was used to minimize fiber damage. However, fiber displacements were still restricted to 30 μm, the load train was highly compliant, and there was no direct observation during the test. One of the primary drawbacks of these limitations was that fiber sliding could not be evaluated.

The current paper describes the design of an apparatus developed specifically for performing elevated temperature fiber push-out tests. This apparatus is capable of achieving fiber displacements up to 1 mm, offers visual monitoring of the tests, and can heat the test specimen up to 1100 °C. The design has the added benefits of being

compact and relatively inexpensive. The capabilities of this apparatus are demonstrated by presenting results for SCS-6 SiC fiber-reinforced Ti–24Al–11Nb (Ti–24–11) and Ti–15V–3Cr–3Sn–3Al (Ti–15–3) matrix composites. The results are discussed in terms of residual stresses, interfacial wear, matrix ductility, and changing modes of interfacial failure.

II. EXPERIMENTAL

A. Fiber push-out apparatus

The fiber push-out test is based on measuring the resisting force at which a fiber opposes the motion of an indenter that is driven by a constant displacement rate mechanism. Load versus time data establish the loads at which fiber debonding and sliding occur. Different methods have been used to achieve this capability. For example, Bright *et al.*[3] showed that an Instron testing machine could be used to control the indenter motion. Eldridge[17] later developed a desktop version of the testing apparatus using a small motorized translation stage instead of an Instron load frame. Further improvements included the addition of video imaging and acoustic emission detection to aid identification of fiber debonding and sliding events.

Extending fiber push-out testing to elevated temperatures required adding the capabilities of sample and indenter heating and providing a nonoxidizing environment. The major requirements that had to be addressed were (i) control of the indenter motion within the test chamber, (ii) fast sample and indenter heating while keeping nearby components cool, and (iii) the capacity to perform fiber/indenter alignment at temperature within the test chamber.

Figure 1 shows a schematic of the elevated temperature fiber push-out apparatus. The sample and indenter are located inside a cubical stainless steel chamber with conflat-flanged ports on each face. This test chamber is evacuated with an attached turbopump that produces a base pressure in the chamber below 1×10^{-6} Torr; this low pressure prevents significant oxidation of the sample during testing at high temperatures.

Controlled indenter displacement is performed using a linear motion feedthrough (Varian Model 954-5150) driven by a stepper motor (Model SX57-102, Compumotor). The indenter/load cell assembly is coupled directly to the shaft of the linear motion feedthrough. The linear motion feedthrough was modified by the addition of a Teflon bushing around the shaft entering the vacuum as well as the incorporation of two thrust washers around the threaded portion of the shaft on the air side. These modifications eliminated both the lateral and vertical play which made the performance of the linear motion feedthrough unacceptable in its unmodified state. During a test, the stepper motor produced a rotational speed

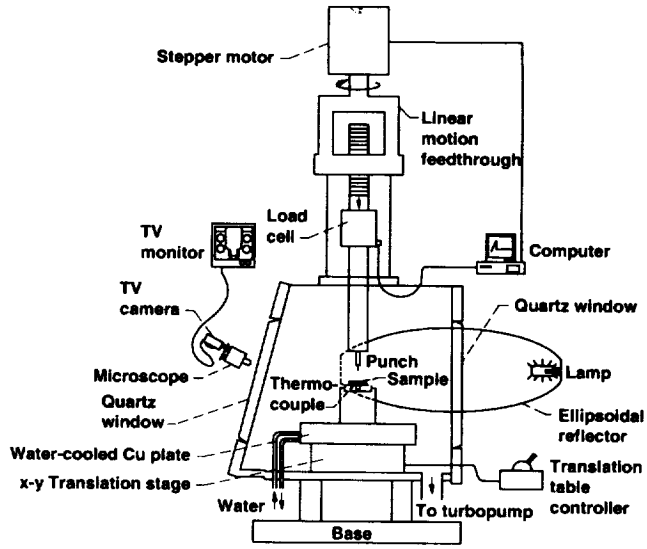

FIG. 1. Schematic diagram of elevated temperature fiber push-out apparatus.

of 0.1 rpm (50 800 microsteps/rev) which translated to 1.06 μm/s linear motion of the indenter.

The indenter used for pushing out fibers is a flat-bottomed cylindrical tungsten carbide punch (National Jet Corp.); a 100 μm diameter punch was used for pushing out the 142 μm diameter SCS-6 SiC fibers. This indenter geometry has the benefits of relatively uniform loading of the fiber end, thereby minimizing fiber damage, and the ability to displace the fiber over long lengths (up to 1 mm) without any contact between the indenter and the matrix. The indenter is coupled through a hollow stainless steel shaft to a load cell.

The sample support fixturing was designed for high-temperature exposure and thermal isolation (Fig. 2). The specimen is mounted with a spring-loaded Inconel clamping device which eliminates the need for adhesives. A set of three 300-μm-diameter channels machined into the top surface of the Ta sample support block allows fibers sitting above those channels to be pushed out without resistance from the support block. The channel width was chosen to be as small as possible to minimize sample bending under the applied load, but large enough to allow a reasonable number of fibers to be tested during one run. Thermal isolation is provided by mounting the Ta sample support block on a low-thermal-conductivity ceramic pedestal which, in turn, is secured to a hollow stainless steel fixture. This assembly is mounted on an x-y translation stage; a water-cooled Cu plate located between the pedestal fixturing and the translation stages prevents the translation stages from overheating (stage temperature never exceeds 30 °C).

Sample heating is achieved using a quartz halogen lamp inside an ellipsoidal reflector (Model 4085, Research Inc.) with the lamp at one focal point and

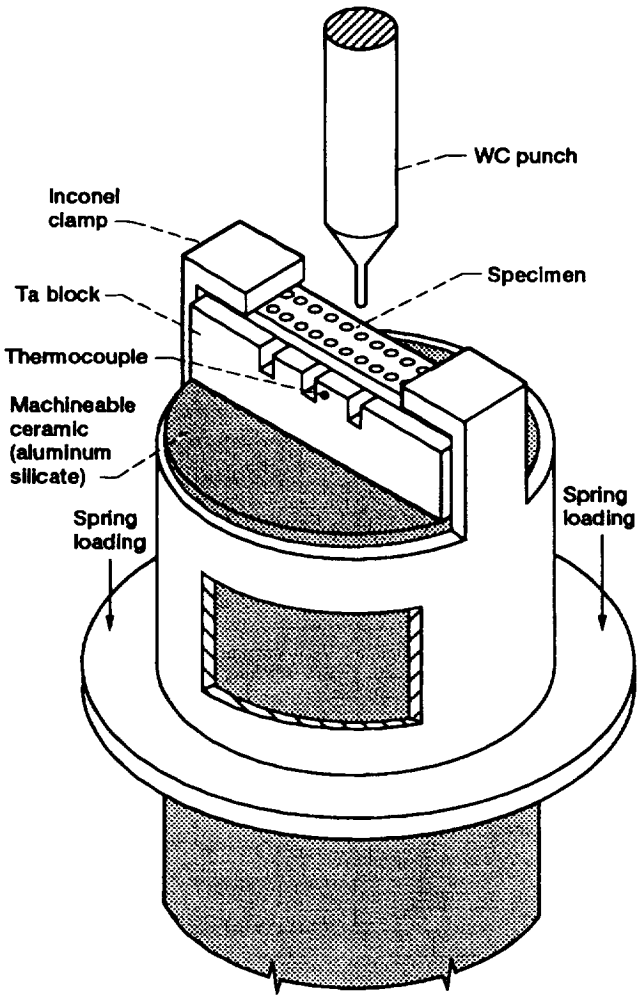

FIG. 2. Enlarged view of specimen support arrangement.

the sample at the other where the heating radiation is focused. The reflector is bisected by the chamber's vertical quartz window, so that the lamp itself remains outside the test chamber. Sample heating to over 1000 °C takes less than 10 min. The hot zone is a spot with a diameter of about 1.25 cm. Sample temperature is monitored by a thermocouple attached to the Ta sample support block.

Fiber/indenter alignment is performed remotely, using motorized translation stages (Model CR4072M stages, Daedal, with Model 18022 Motor Mike Drives, Oriel) to bring an individual fiber beneath the indenter. A quartz window tilted at an angle of 25° from vertical provides line-of-sight for a long-working-distance optical microscope positioned outside the chamber. The microscope is positioned so that the line-of-sight is perpendicular to the plane of the window, minimizing image distortion and multiple reflections. Satisfactory fiber/indenter alignment is evaluated by watching the video image of the indenter above the sample. A recessed version of the tilted quartz window has recently been substituted for the original window, now allowing positioning of the microscope objective to within 5 cm of the sample.

A PC-controlled data acquisition system (System 575, Keithley Instruments) is used to collect data. Load and time are monitored, displayed on screen both numerically and graphically as they are acquired, and stored on floppy disk. In addition to data acquisition, the PC controls the motion of the indenter via RS-232 communication with the stepper motor controller.

In situ video monitoring of the test displays the view from the optical microscope overlaid with a real-time PC-generated plot of the load versus time data. Video tape recording of this display provides a method of correlating events from the fiber push-out load versus time curves with observable events occurring on the TV image. The videotape can be replayed, and the operator can confirm whether a load drop corresponded to initial fiber movement, or, for example, a matrix crack.

All fiber push-out tests were performed as described above except for room-temperature measurements, which for convenience, were performed on a previously developed desktop fiber push-out apparatus.[17]

B. Materials

The composite materials tested were a unidirectional SCS-6 SiC fiber (Textron Specialty Materials) reinforced Ti–24Al–11Nb (Ti–24–11) prepared by a powder cloth process at NASA Lewis and a unidirectional SCS-6 SiC fiber-reinforced Ti–15V–3Cr–3Sn–3Al (Ti–15–3) prepared by a foil consolidation process by Textron Specialty Materials. Thin specimens of the composites were cut with a diamond saw perpendicular to the fiber axes and then mechanically polished down to a 1 μm finish using diamond lapping film. Final specimen thicknesses ranged from 0.28 to 0.48 mm. The specimen was then secured by its ends with the spring-loaded clamp onto the support block/heat isolation platform assembly. An optical micrograph was taken of the mounted specimen; the fibers aligned above the channels in the support block were then indexed on the micrograph for subsequent testing. The mounted specimen was then inserted into the test chamber.

III. RESULTS

A. Fiber push-out

Figure 3 shows average interfacial shear stress, τ_{av}, versus feedthrough displacement for representative push-out tests at different temperatures. Feedthrough displacement is equivalent to the crosshead displacement of a universal testing frame, and has been labeled as such for comparison with previous work. The average interfacial shear stress, τ_{av}, is the applied load, P, divided by the

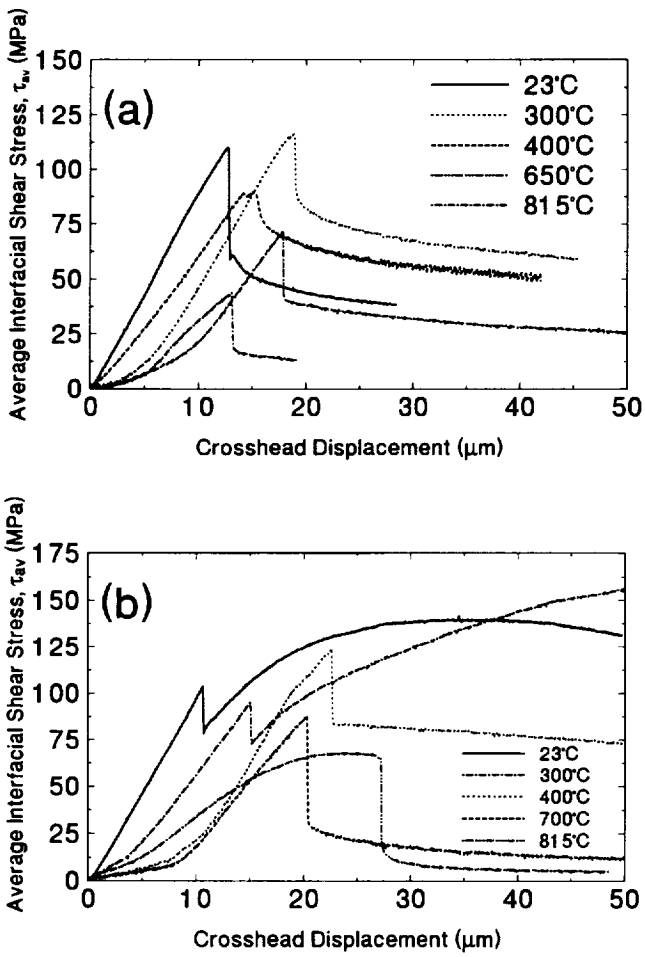

FIG. 3. Representative fiber push-out τ_{av} versus displacement curves at different temperatures. (a) SCS-6/Ti-24-11, and (b) SCS-6/Ti-15-3.

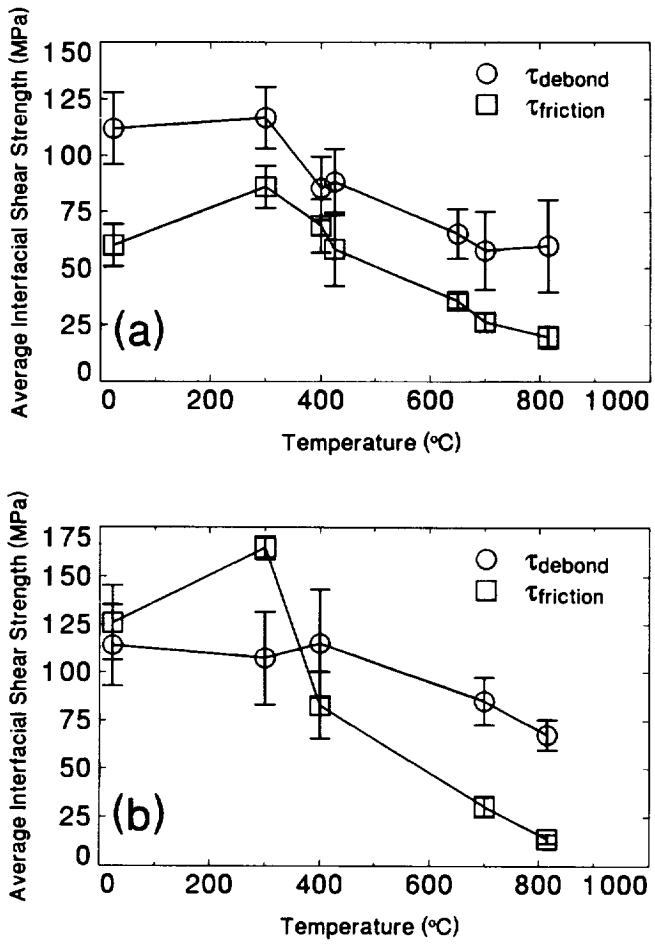

FIG. 4. Average τ_{debond} and $\tau_{friction}$ versus temperature. (a) SCS-6/Ti-24-11, and (b) SCS-6/Ti-15-3.

contact area between fiber and matrix, $\pi d_{fiber} t$, where d_{fiber} is the fiber diameter and t is the sample thickness. It was shown earlier[18] for SCS-6/Ti-24-11 at room temperature that, over the range of sample thicknesses used here, τ_{av} has no significant thickness dependence and can be used to compare results from samples of different thicknesses. Most of the curves consisted of an initial monotonically increasing portion followed by a sharp drop at debonding. The shear stresses after debonding, which correspond to purely frictional resistance, usually showed slowly decreasing values. The push-out measurements for SCS-6/Ti-15-3 at 23 and 300 °C were exceptions in that they showed a continuous increase in τ_{av} with continued fiber displacement until a maximum was reached at relatively long displacements.

Averages with standard deviations accumulated from testing many fibers are summarized in Fig. 4 which shows plots of τ_{debond} (maximum τ_{av} before debonding) and $\tau_{friction}$ (τ_{av} immediately after debonding, except for SCS-6/Ti-15-3 at 23 and 300 °C where the peak value after debonding was taken) versus temperature. In both cases, τ_{debond} does not decrease significantly until relatively high temperatures. Note that, as defined, τ_{debond} and $\tau_{friction}$ are average stresses, and thus, do not necessarily accurately reflect local stresses along the interface.

SEM observation of pushed-out fibers was also performed. Examination of SCS-6 fibers pushed out of Ti-24-11 showed that interfacial failure always occurred between the C-rich coating and the reaction zone, and that there was little coating damage at any temperature. In contrast, examination of SCS-6 fibers pushed out of Ti-15-3 showed a variety of locations of interfacial failure, including within the C-rich coating, between the fiber and the coating, and very rarely between the coating and reaction zone. The difference in locations for interfacial failure between the Ti-24-11 and Ti-15-3 matrix composites was probably due to two factors. First, the rougher coating/reaction zone interface in the Ti-15-3 matrix composite would tend to prevent sliding at that interface. Second, more fiber coating was consumed during processing of the Ti-24-11

matrix composite to the extent that only the inner layer of the duplex SCS-6 coating survived,[4] making intracoating failure less likely in the Ti–24–11 matrix composite. In contrast to the Ti–24–11 matrix composite, there was a marked temperature dependence in the interfacial wear for the Ti–15–3 matrix composite. Fibers pushed out at 23 °C showed severe fracturing of the C-rich coating with coating debris accumulation at the fiber/matrix interface, while fibers pushed out at 815 °C showed no significant damage (Fig. 5).

B. Fiber push-back

Fiber push-back tests were also performed in an attempt to decouple the contribution from interfacial roughness to the sliding frictional stress. In these tests, fibers were pushed out in one direction, the sample was flipped over, and the same fibers were pushed back in the opposite direction. The push-back load/displacement curves (Fig. 6) typically showed a load minimum as the fiber moves through its initial undisplaced position. This previously described phenomenon[19–21] occurs because the initial undisplaced position is the only fiber position where the contacting fiber and matrix surfaces are in perfect registry.

Two sets of fiber push-back tests were performed on SCS-6/Ti–24–11. The first set consisted of doing all the initial fiber push-outs at room temperature and then pushing the fibers back at the selected temperature. The second set consisted of performing all the initial fiber push-backs and the subsequent push-backs at the same selected temperature. The load minimum for each push-back was recorded and converted to an average shear stress; these data are summarized in Fig. 7 along with the post-debond frictional shear stresses already presented in Fig. 3(a).

IV. DISCUSSION

The capability of the newly developed elevated temperature fiber push-out apparatus is well demonstrated by Figs. 3 and 4. Temperature dependencies of shear stresses at fiber debonding and during fiber sliding are shown. Work is underway to obtain a more complete understanding of these changes in terms of calculated stress distributions along the length of the interface,[22] but for this report, the results are interpreted in terms of average shear stresses, which are much more easily reducible from the loads.

A. Fiber debonding

The absence of any significant decrease in the average shear stress at debonding until beyond 300 °C for SCS-6/Ti–24–11 and beyond 400 °C for SCS-6/Ti–15–3 indicates that the large reductions in residual shear and radial stresses that occur upon heating to those temperatures do not affect the loads at which fiber

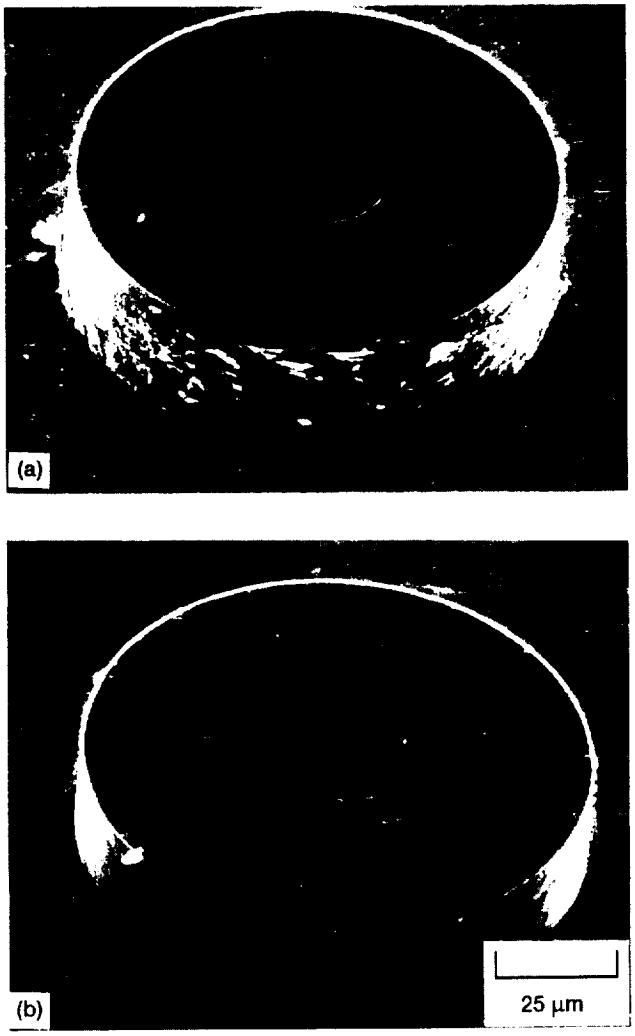

FIG. 5. SEM micrographs of SCS-6 fibers pushed out of Ti–15–3 matrix. (a) 23 °C, and (b) 815 °C.

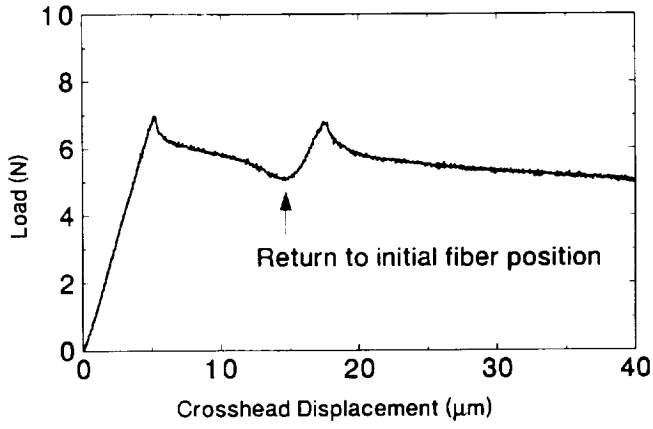

FIG. 6. Representative fiber push-back load versus displacement curve for 0.32 mm thick SCS-6/Ti–24–11 at 23 °C.

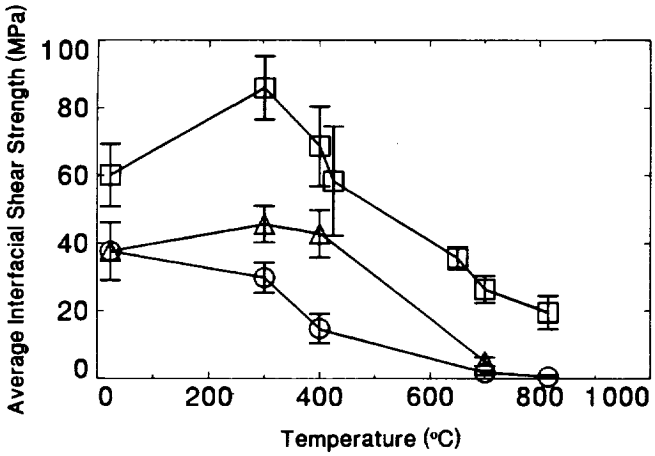

FIG. 7. τ_{av} during frictional sliding versus composite temperature. (□) Post-debond friction from Fig. 3(a). (○) Friction at push-back minimum; initial push-out at room temperature. (△) Friction at push-back minimum; initial push-out at same temperature as push-back.

debonding occurs. This is contrary to the expectation that reduced residual shear stresses will cause reductions in the fiber debonding loads.[11,23] At higher temperatures, the observed decrease in average shear stress at debonding may be due to two factors. One possibility is that the location of the maximum total shear stress (site of mode II debond initiation) may change from the bottom of the sample at low temperatures to the top at high temperatures.[22] This change in location (see Fig. 8) could occur because the residual shear stresses tend to offset the shear stresses induced by the indenter loading near the topface (suppress debonding), but add to the somewhat attenuated indenter-induced stresses at the bottomface (promote debonding), favoring debond initiation near the bottomface at lower temperatures. At high temperatures, however, the residual stresses are small so the maximum shear stress will be where the indenter-induced shear stresses are highest, which is near the topface. The second possibility is that, at higher temperatures, the residual clamping stresses may be sufficiently reduced to allow mode I debonding to occur at the backface.[24,25] However, there was no direct evidence from SEM observation of tensile crack opening along the fiber circumference.

B. Fiber sliding

The frictional sliding stresses are presumed to follow the relationship:

$$\tau_{\text{friction}} = \mu\sigma_r, \tag{1}$$

or the more general form:

$$\tau_{\text{friction}} = \tau_0 + \mu\sigma_r, \tag{2}$$

where τ_0 is a constant, nonCoulombic component of shear stress, μ is the coefficient of friction, and σ_r is

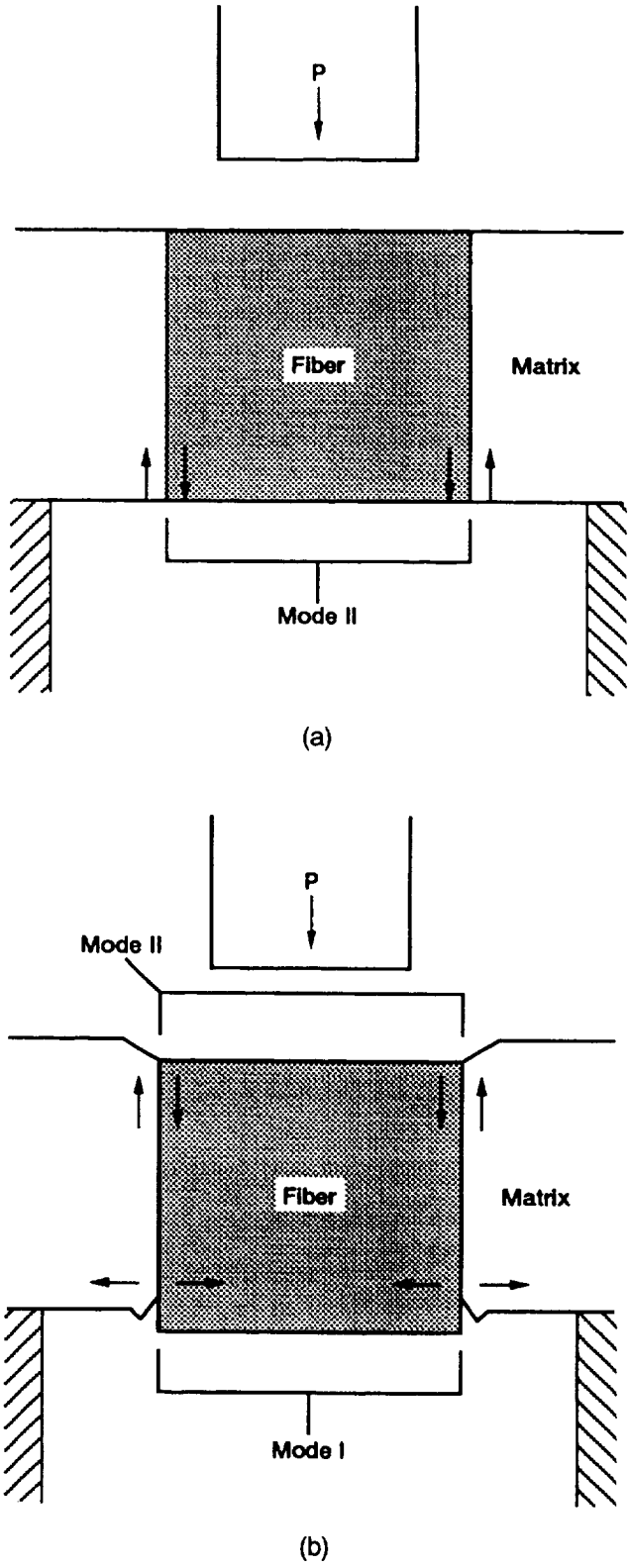

FIG. 8. Proposed debond initiation sites for thin-slice fiber push-out specimens with $\alpha_m \gg \alpha_f$.[22] (a) Low temperature, mode II debonding at bottomface; (b) high temperature, mode II debonding at topface and/or mode I debonding at bottomface. Possible matrix yielding.

the radial stress at the interface. Before being displaced, σ_r is due solely to the residual stresses produced when the sample was cooled from fabrication temperature. The residual radial stresses arise from the thermal expansion misfit[23,26]:

$$\sigma_r = \frac{qE_fE_m}{E_m(1 - \nu_f) + E_f(1 + \nu_m)}\Delta\alpha\Delta T, \quad (3)$$

where E_f, E_m, ν_f, and ν_m are the elastic moduli and Poisson's ratios of the fiber and matrix, respectively, q is a factor that adjusts for the fiber volume fraction ($q = 1$ for an infinite single fiber composite), and $\Delta\alpha\Delta T$ is the thermal expansion misfit strain for an infinite single fiber composite. The average frictional shear stresses measured in the fiber push-out test, however, are for a displaced fiber. While Eqs. (1) and (2) will still hold, Eq. (3) neglects the changes in σ_r which occur after the fiber is displaced from its initial undisplaced position. These changes are due to the added mismatch strain due to the contacting irregular fiber and matrix surfaces being out of registry as well as changes in interface roughness caused by interfacial wear during fiber sliding. Fiber push-back tests allow measurement of frictional stresses at the undisplaced fiber position where the fiber and matrix surfaces are back in registry. However, due to the irreversible nature of interfacial wear, the pristine interface condition is never completely achieved during push-back and Eq. (3) is only a good approximation for σ_r at the push-back reseating if there is little interfacial wear.

The effects of temperature on frictional sliding stresses are observed in the fiber push-out results. Figure 4 shows that τ_{friction} has a general downward trend with increasing temperature, consistent with the expected decrease in σ_r with temperature [Eqs. (1)–(3)]. However, the observed frictional sliding behavior cannot be explained completely by reductions in the thermomechanical clamping stresses given by Eq. (3). For example, the results for SCS-6/Ti–24–11 show an increase in τ_{friction} up to 300 °C even though there should be a substantial decrease in residual clamping stresses compared to room temperature. This can be explained only by differences in interfacial wear that change interface roughness. The fiber and matrix surfaces in contact may experience more severe wear at lower temperatures where fiber sliding occurs under higher radial compressive stresses.

In contrast, fiber push-back measurements where the initial push-outs were all performed at room temperature (Fig. 7) show a steady decrease in frictional shear stress all the way to zero with increasing temperature. These push-back results give a better relative indication of σ_r, not only because the measurements are obtained at the initial undisplaced fiber position, but also because all the initial forward pushes were performed at room temperature where the maximum amount of fiber and matrix smoothing from interfacial wear occurs, thereby equalizing the interfacial roughness for subsequent push-backs. Further support of the greater wear of the fiber and matrix surfaces at room temperature is given by comparing these results to those obtained where the initial push-outs were performed at the same temperature as the subsequent push-backs (Fig. 7). In this case, there is no significant decrease in frictional shear stress with increasing temperature until above 400 °C; this can be ascribed to the greater interfacial wear occurring at lower temperatures. The decrease in τ_{friction} to nearly zero at 700 °C in both sets of push-back tests indicates that $\tau_0 = 0$ [Eq. (1)] at the undisplaced fiber position. Thus, the nonzero τ_0 associated with frictional measurements for a displaced fiber is entirely due to the additional pressure created by the irregular fiber and matrix surfaces being out of registry. This supports the claim by Mackin *et al.*[20] that the frictional shear stress is entirely Coulombic despite the presence of a constant τ_0 contribution.

The push-out curves for SCS-6/Ti–15–3 show a much more evident temperature-dependent wear behavior [Fig. 3(b)]. At room temperature and 300 °C there is an increase in frictional shear stress with continued fiber sliding after debonding. This increase was associated with fracturing of the fiber coating with coating debris accumulation at the interface [Fig. 5(a)] which would impede further fiber sliding. This type of frictional sliding behavior has been observed previously at room temperature,[21,27,28] and is common when debonding occurs at more than one interface. The loss of coating integrity precluded the meaningful use of push-back testing for this composite. Severe coating fracturing was not apparent for tests at higher temperature [Fig. 5(b)], where fiber sliding occurs without increasing frictional resistance; this indicates coating fracturing is less prevalent when fiber sliding occurs under lower levels of radial clamping stress, σ_r.

V. CONCLUSIONS

An apparatus for elevated temperature fiber push-out testing has been successfully designed and assembled. This apparatus measures the force at which a fiber resists the motion of a flat-bottomed indenter driven at constant speed. Temperature (up to 1100 °C) and vacuum environment (10^{-6} Torr) are maintained while controlling indenter motion and sample position. In addition, real-time video monitoring of the test is provided.

The average shear stress at fiber debonding for SCS-6/Ti–24–11 and SCS-6/Ti–15–3 does not decrease until beyond 300 °C. This lack of temperature dependence suggests that decreases in residual shear and radial stresses do not affect fiber debonding until either (1) the reduction in residual shear stresses changes the *location* of the maximum shear stress (initiation point

of mode II debonding) from the bottom to the top of the sample or until (2) the residual radial compressive stresses are reduced to the point where a tensile (mode I) crack opening at the interface can be induced at the bottom of the sample by bending stresses. A better understanding of the interfacial failure progression will require modeling of the stress component distributions along the length of the interface.

Frictional shear stresses were found to reflect reduced residual clamping stresses with increasing temperature, but were sometimes dominated by changes in interfacial wear. A fiber push-back technique was found to give frictional measurements without the out-of-registry component of compressive radial stress due to interfacial roughness. The decrease of the remaining residual clamping stress to zero at an elevated temperature suggests that the frictional stress is entirely Coulombic.

ACKNOWLEDGMENTS

The authors wish to thank D. Dixon for his skillful assistance in the design and assembly of the testing apparatus. Thanks are also due to S. Pepper, R. Bhatt, and L. Westfall for their helpful discussions on the apparatus design, A. Korenyi-Both for SEM analysis, and to P. Brindley and P. Kantzos for providing the composite materials.

REFERENCES

1. D. B. Marshall, J. Am. Ceram. Soc. **67** (12), C258 (1984).
2. D. B. Marshall and W. C. Oliver, J. Am. Ceram. Soc. **70** (8), 542 (1987).
3. J. D. Bright, D. K. Shetty, C. W. Griffin, and S. Y. Limaye, J. Am. Ceram. Soc. **72** (10), 1891 (1989).
4. J. I. Eldridge and P. K. Brindley, J. Mater. Sci. Lett. **8** (12), 1451 (1989).
5. C. J. Yang, S. M. Jeng, and J-M. Yang, Scripta Metall. Mater. **24**, 469 (1990).
6. T. P. Weih and W. D. Nix, J. Am. Ceram. Soc. **74** (3), 524 (1991).
7. M. C. Watson and T. W. Clyne, Acta Metall. Mater. **40** (1), 141 (1992).
8. A. G. Evans, F. W. Zok, and J. Davis, Comp. Sci. Technol. **42**, 3 (1991).
9. W. A. Curtin, J. Am. Ceram. Soc. **74** (11), 2837 (1991).
10. H. M. Chou, M. W. Barsoum, and M. J. Koczak, J. Mater. Sci. **26**, 1216 (1991).
11. D. B. Marshall, M. C. Shaw, and W. L. Morris, Acta Metall. Mater. **40** (3), 443 (1992).
12. Y. Le Petitcorps, R. Pailler, and R. Naslain, Comp. Sci. Technol. **35**, 207 (1989).
13. J. Aveston, G. A. Cooper, and A. Kelly, in *The Properties of Fibre Composites*, Conference Proceedings (IPC Science and Technology Press Ltd., Teddington, U.K., 1971), p. 15.
14. B. N. Cox, M. S. Dadkhah, M. R. James, D. B. Marshall, W. L. Morris, and M. Shaw, Acta Metall. Mater. **38** (12), 2425 (1990).
15. G. Morscher, P. Pirouz, and A. H. Heuer, J. Am. Ceram. Soc. **73** (3), 713 (1990).
16. M. K. Brun, J. Am. Ceram. Soc. **75** (7), 1914 (1992).
17. J. I. Eldridge, Desktop Fiber Push-Out Apparatus, NASA TM 105341 (1991).
18. J. I. Eldridge, in *Intermetallic Matrix Composites II*, edited by D. B. Miracle, D. L. Anton, and J. A. Graves (Mater. Res. Soc. Symp. Proc. **273**, Pittsburgh, PA, 1992), p. 325.
19. P. D. Jero, R. J. Kerans, and T. A. Parthasarathy, J. Am. Ceram. Soc. **74** (11), 2793 (1991).
20. T. J. Mackin, P. D. Warren, and A. G. Evans, Acta Metall. Mater. **40** (6), 1251 (1992).
21. J. I. Eldridge, R. T. Bhatt, and J. D. Kiser, Ceram. Eng. Sci. Proc. **12** (7–8), 1152 (1991).
22. L. J. Ghosn, P. Kantzos, J. I. Eldridge, and R. Wilson, in *HITEMP Review 1992*, Vol. 2, NASA CP-10104 (1992), p. 27-1 to 27-12.
23. R. J. Kerans and T. A. Parthasarathy, J. Am. Ceram. Soc. **74** (7), 1585 (1991).
24. D. A. Koss, M. N. Kallas, and J. R. Hellmann, in *Intermetallic Matrix Composites II*, edited by D. B. Miracle, D. L. Anton, and J. A. Graves (Mater. Res. Soc. Symp. Proc. **273**, Pittsburgh, PA, 1992), p. 303.
25. M. N. Kallas, D. A. Koss, H. T. Hahn, and J. R. Hellmann, J. Mater. Sci. **27**, 3821 (1992).
26. H. J. Oel and V. D. Frechette, J. Am. Ceram. Soc. **69** (4), 342 (1986).
27. P. Kantzos, J. Eldridge, D. A. Koss, and L. J. Ghosn, in *Intermetallic Matrix Composites II*, edited by D. B. Miracle, D. L. Anton, and J. A. Graves (Mater. Res. Soc. Symp. Proc. **273**, Pittsburgh, PA, 1992), p. 135.
28. I. Roman and P. D. Jero, in *Intermetallic Matrix Composites II*, edited by D. B. Miracle, D. L. Anton, and J. A. Graves (Mater. Res. Soc. Symp. Proc. **273**, Pittsburgh, PA, 1992), p. 337.